



Journal of Mining and Environment (JME)

journal homepage: [www.jme.shahroodut.ac.ir](http://www.jme.shahroodut.ac.ir)



## Robust Principal Component Analysis and Fractal Methods to Delineate Mineralization-Related Hydrothermally-Altered Zones from ASTER Data: A Case Study of Dehaj Terrain, Central Iran

Narges Habibkhah<sup>1</sup>, Hossein Hasani<sup>1</sup>, Abbas Maghsoudi<sup>1</sup> and Mehdi Honarmand<sup>2</sup>

1- Department of Mining and Metallurgical Engineering, Amirkabir University of Technology, Tehran, Iran

2- Institute of Science and High Technology and Environmental Sciences, Graduate University of Advanced Technology, Kerman, Iran

### Article Info

Received 27 April 2020

Received in Revised form 7 September 2020

Accepted 7 September 2020

Published online 16 November 2020

DOI: [10.22044/jme.2020.9619.1876](https://doi.org/10.22044/jme.2020.9619.1876)

### Keywords

Robust principal component analysis

Value-pixel fractal model

Hydrothermal alteration

Porphyry copper

### Abstract

The Dehaj area, located in the southern part of the Urumieh-Dokhtar magmatic belt, is a well-endowed terrain hosting a number of world-class porphyry copper deposits. These deposits are all hosted in an acidic to intermediate volcano-plutonic sequence greatly affected by various types of the hydrothermal alterations, whether argillic, phyllic or propylitic. Although there are a handful of hitherto-discovered porphyry copper deposits in the area, the geological setting of the area suggests the possibility of finding further deposits. The recognition and delineation of the hydrothermal alterations can pave the way for the discovery of further potential zones that possibly host the porphyry copper deposits. The current work proposes a hybrid methodology applied to the Advanced Spaceborne Thermal Emission and Reflection Radiometer (ASTER) imagery by combining the application of dimension reduction and fractal techniques to delineate the hydrothermally-altered zones. In order to reduce the dimensionality of multi-band ASTER data, Robust Principal Component Analysis (RPCA) was employed to elicit the traces of hydrothermally-related mineral assemblages including illite, sericite, quartz, kaolinite, epidote, and chlorite. Highlighting the existence of the aforementioned minerals, the extracted components require interpretation, i.e. a boundary is required to constraint the hydrothermally affected zones from the rest of the geological units. In order to tackle such a challenge, the authors introduce the concept of value-pixel fractal technique for the extracted principal components. The Prediction-Area (P-A) plot is used for the validation, which shows that the identified alterations correlate with the mineralization. The results obtained are verified by a geological survey, where a number of samples are collected from the delineated zones. The samples are analyzed by the XRD techniques, finding that this work is successful in classifying the hydrothermally-altered zones.

### 1. Introduction

The necessity to discover further mineral resources is of paramount importance, which has caused the exploration geologists to apply various techniques for delimiting the areas that are favorable for the detailed exploration surveys. The applied techniques are constrained by the type of deposits for which the exploratory surveys are conducted and the zone in which the surveys are carried out. The objective of this work was to define an exploratory criterion for discovering the

porphyry copper deposits in Dehaj terrain, located in the southern part of the Urumieh Dokhtar Magmatic Belt (UDMB) in the Kerman Province. This belt is often regarded as a major metallic province endowed with Cu, Mo, and Au minerals [1-5]. This copper-endowed metallic province hosts a plethora of porphyry copper deposits (e.g. [6-17]). These deposits are often accompanied by extensive halos of hydrothermal alterations, especially the propylitic, phyllic, and argillic

alterations [18]. These vast alteration zones can be recognized by the remote sensing (RS) techniques, and this is the goal for which the authors conducted this work.

Many studies have been conducted on these deposits in order to identify the altered areas utilizing RS (e.g. [8, 11, 14, 16, 17, 19, and 20]). Different methods such as band ratios and principal component analysis have been used to separate the alteration zones. On a regional scale, a few studies have been done such as applying the band ratio for mapping the alteration zones [3], using the PCA and SAM methods for investigating the alteration zones, and separating the potential mineralization into two groups (high and low) [4, 5, and 21]. Although these methods are successful, they do not clearly distinguish between the alterations. While understanding these zones is vital for discovering the areas of high anomaly, the aforementioned studies have paid little attention to separate the alteration zones and extract their specific minerals. This work serves as the dual purposes of investigating the hydrothermal alteration and identifying the high intensity of various alterations to enhance the accuracy of the work.

The Advanced Space borne Thermal Emission and Reflection Radiometer (ASTER) has been frequently used to recognize the alteration zones (e.g. [2-4, 22-26]). Nevertheless, application of the ASTER imagery data for delineation of the hydrothermal alteration zones is not without error. First, the availability of different bands poses serious challenges to a proper recognition of the alterations. Secondly, the boundary between the altered and fresh zones remains uncertain, which is a crucial factor in the exploration of the porphyry copper deposits.

This work endeavors to address the above-mentioned challenges through a hybrid approach by combining the dimension reduction and classification techniques. The former challenge is addressed by the application of the robust principal component analysis (RPCA) as a dimension reduction method different from the ordinary principal component analysis (PCA), which leaves a number of components, and portrays the distribution of the targeted minerals. The latter challenge, however, is tackled by the application of the proposed fractal technique. Developed from the number-size model proposed by Mandelbrot [21, 27], this technique is based on the pixel values and their statistical and spatial distribution. Application of the proposed value-

pixel method classifies the alteration zones with respect to their intensity.

The results obtained were verified by a number of samples collected from the delineated zones and analyzed by XRD. These suggest the reliability of the proposed methodology.

## 2. Geological Setting

Located in the southern part of the Urumieh-Dokhtar magmatic belt (UDMB) (Figure 1a), the Dehaj terrain covers an area of ~5900 km<sup>2</sup>. The area has been subjected to different successions of volcanism that commence from early Eocene with the emplacement of basic to acidic volcanic sequence (Figure 1b). The volcanic activities in the area continued in Oligocene, bringing about the development of large batholiths and small dykes with the dioritic composition. The intrusive rocks acting as the heat source and the source of mineral-bearing fluids are inextricably linked with the porphyry copper mineralization [28, 29]. Magmatism lasted until Quaternary with the deposition of basic extrusions comprising basalts and andesite basalts. There are various types of volcano-sedimentary and sedimentary formations outcropping in the area with their age varying from Cretaceous to Quaternary. They include the colored mélanges, Cretaceous sedimentary rocks, Miocene sedimentary sequence, and Quaternary alluvial fans [30, 31].

The mineralization processes occurring in this area are divided into the hypogene and supergene steps. The primary mineralization caused by the magmatic and hydrothermal fluids has been formed in the stock works that are saturated with iron, malachite, and azurite alterations. Most abundant supergene minerals consist of pyrite, chalcopyrite, and bornite. In another type of mineralization, the fluids penetrated into the ground have played a vital role in emerging new minerals. These fluids have oxidized the sulfidic zone and produced the products such as digenite and chalcocite [32, 33].

The potassic, phyllic, argillic, and propylitic alterations indicate the existence of hydrothermal activity in the studied area. The potassic zone is characterized by the biotite alteration among the intrusive quartz-monzonite and monzodiorite bodies. The phyllic alteration, to which a huge part of the area is assigned, alters both the intrusive body and host rock. This alteration occasionally covers other alterations, and has a composition of sericite and secondary quartz. Some regions of the area, especially the Eocene

volcanic rocks, have survived the clay alteration. According to the microscopic studies, the maximum effect of clay alteration has been produced on plagioclase, biotite, and hornblende, causing the chloritization. In the south part of the region, the high intensity of the argillic mineral

makes it easier to distinguish between the oxide and hydroxide iron concentrations. The propylitic alteration in the studied area appears as the holes filled with calcite, chlorite, and epidote with an important exploratory perspective [29, 30].

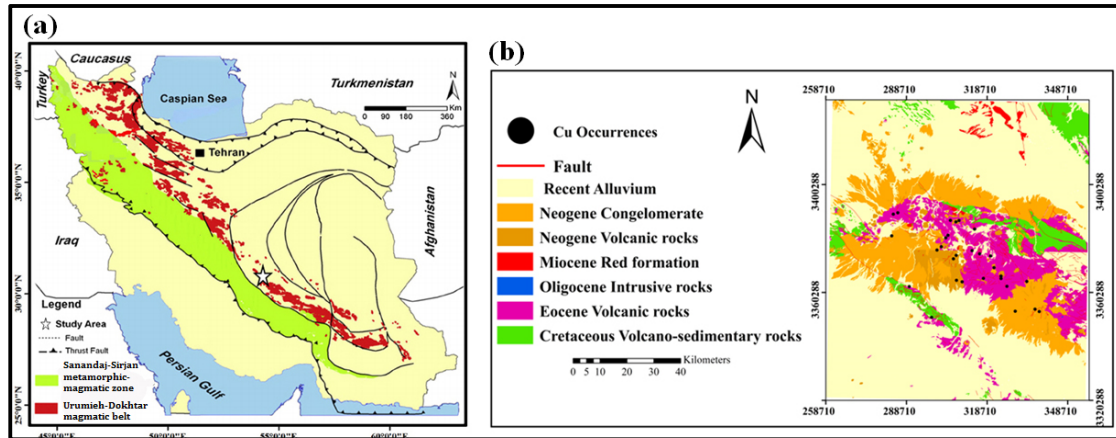


Figure 1. (a) The location of the study area in Map of structural zones of Iran [34], (b) The simplified regional geologic map of the study area which is classified by age [28]

### 3. Materials and method

#### 3.1. ASTER data

In this work, a 1B level scene of the Aster imagery data taken on 12.8.2001 from the Earth Remote Sensing Data Analysis Center (ERSDAC) was used. ASTER is a multi-spectral sensor comprising 14 bands that cover the wavelength range of 52-11.65  $\mu\text{m}$  with three spectral ranges including visible and near infrared: (VNIR: 1 to 3 bands), six short-wave infrared bands (SWIR: 4 to 9 bands), and five thermal infrared bands (TIR: 10 to 14 bands). The data was utilized for a series of pre-processing techniques. They were atmospheric, radiometric, and geometric corrections applied using the ENVI and the ASTER Correction Tool software package, respectively [35].

#### 3.2. Image processing

Ordinary principal component analysis (PCA) is a dimension reduction technique that has been applied in different areas [36]. PCA is a powerful statistical technique that can be used to compress images and eliminate the unwanted effects. It is based on the principle that the axes shift in the direction that represents the maximum variability. This technique summarizes the variability of complex datasets, and has gained an unprecedented popularity in the remote sensing studies (e.g. [2, 22, 37, 38, 39, and 40]). The data

is transformed to a number of uncorrelated principal components (PCs) using the correlation or covariance matrices [41]. The relationship between the variables (different bands) and PCs is represented by a loading matrix. A positive loading shows a positive relationship between the bands and PCs, and vice versa [42, 43]. The relationship between PCs and different pixels is represented by the PC scores or the images' digital values [44].

The data for various bands often correlate. The correlation between the images of the bands demonstrates that there is some common information or, in other words, they have a repeated information. The transformation of the principal component is a method to remove or reduce such ancillary information, which is done by compressing the multi-spectral data into a new coordinate system. The information in the multi-spectral bands is often less than the number of bands, and therefore, the objective of PCA is to determine the number of dimensions in an information collection [42, 43, and 45]. In order to calculate PCA, the variance-covariance matrix or the correlation matrix is first constructed. Then the eigenvalues of this matrix are calculated. Since the covariance depends on the data measurement unit and the different bands do not have the same reflective information, it is better to use the correlation matrix [41]. After identification of the absorptive and reflective

bands of each mineral, the specific image for that mineral can be obtained. It should be noted that if the reflective band is positive, the bright pixels are the target area; otherwise, the dark pixels are so [38]. The results of this method are more obvious than those of the raw images.

Crosta [38] has proposed a method called the “Crosta” technique. This is a new simple technique for mapping the alterations. In this method, only the preliminary information is required for the spectral properties of minerals and plant [46]. The difference between the standard and selective analyses is that in the standard analysis, all the bands in an image are used as the input data, whereas in the selective analysis, a certain number of bands are selected based on the type of target [12, 47]. In the Crosta analysis, those bands are selected that have certain reflection and absorption features in each mineral [48]. Reducing the number of input bands leads to the increased detection of a unique PCA for a certain mineral.

Although PCA has been successfully applied to an array of remote sensing studies (e.g. [22, 41, 43, and 49]), it suffers from a major drawback: the extreme values render the extracted components biased [50]. The robust principal component analysis (RPCA), however, has been developed to tackle the mentioned drawback [51]. In this method, a minimum covariance determinant estimator is used instead of the correlation or covariance matrices [52]. This method has been explicitly explained in [51, 53], not warranting further explanations.

Each mineral shows either an absorptive or a reflective behavior in a multi-band spectrum range. According to these features, RPCA can be used to extract the traces of key minerals using a selective approach proposed in [22]. The number of input bands is subjectively selected by the user, which reduces the noises affecting the output [38]. In this work, we applied the same logic for extracting the traces of hydrothermal alteration-related minerals using RPCA and estimated a good model for the background variations.

### 3.2.1. Robust principal component analysis (RPCA)

The RPCA method is performed aiming to compress the massive data in different bands of an image and to remove the identical data. RPCA is very important for interpreting the digital remote-sensing data. The most important advantages of the RPCA method are the collection and

compression of data on the phenomena in different bands into a smaller number of bands or components. In other words, this method is widely used to remove the redundant satellite data [54].

The output of this method is usually a number of new limited bands between which the correlation is minimized, which are independent from each other and therefore, they can be interpreted as independent from the original data. In the satellite images, there is usually a correlation (from very weak to very strong) between the multi-spectral bands, especially the adjacent bands. The RPCA method is relevant to a multivariate analysis that can be used to transfer a series of multi-spectral images in such a way that the new components do not correlate with each other and are arranged in a way that they can describe the differences in the images. In this way, these components show the inherent differences of the main bands in a statistical and compressed manner. In fact, RPCA is a statistical method that is used to reduce the redundant data and convert the multi-band data into fewer components. The principal components can be used to compress the data contained in a number of bands. As such, there will be maps with complete and concise data, and the analysis of the new images is more accurate than that of the raw images. It also greatly reduces the time and cost of performing the task. Normally, the initial image obtained by this method can collect 0.80 of data (the most accurate image) and the subsequent images have less data, respectively. Due to the variance of the data in the components and the unique nature of the data in each component, this method can be used to retrieve and detect the changes. When there are more than two bands, it is more complex to transfer the principal component axes. Considering the variance-covariance matrix whose components represent the variance and covariance between the two bands I and J of the image, its values can be obtained [55, 56]. For retrieving and detecting the changes using the principal component analysis, the multi-spectral images prepared at different times are considered a dataset on which the principal component analysis operations are performed. In this process, the change data is displayed in several components, the number of which can vary depending on the changes in the region. Therefore, the change data is distributed in several components, and it is difficult to identify which component is considered to detect the changes in a phenomenon and is required to be investigated. In other words, distribution of the

change data in several components is one of the major limitations of this method.

RPCA decomposes a given matrix into the background and sparse matrices [56].

$$M = L_0 + S_0 \quad (1)$$

In this equation,  $M$  is a data matrix and  $L_0$  and  $S_0$  are the low-rank and sparse ones, respectively ( $L$ ,  $S$ , and  $M \in \mathbb{R}^{m \times n}$ ).

It can be described mathematically as follows:

$$\min_{L,S} \|L\|_* + \lambda \|S\|_1 \text{ s.t: } M = L_0 + S_0 \quad (2)$$

where  $\|L\|_* = \sum_r \sigma_r(L)$  define the nuclear norm of  $L$ ,  $\sigma_r(L)$  ( $1, 2, \dots, \min(m, n)$ ) is the  $r^{\text{th}}$  singular value of  $L$ ,  $\|S\|_1 = \sum_{ij} |e_{ij}|$  denotes the  $L_1$ -norm of  $S$ , and  $e_{ij}$  is the element in the  $i^{\text{th}}$  row and  $j^{\text{th}}$  column of  $S$  [56]. RPCA has been applied to machine learning.

### 3.3. Value–Pixel fractal model

The fractal self-similarity approaches can be applied in order to recognize the data having a number of similar features [57]. In other words, these methods can be applied to classify a dataset that shows variability [43]. These techniques have been applied in the earth sciences for a variety of purposes [21, 31, 58, 59, and 60].

The remote sensing-based imagery includes various pixels with different digital values. The pixels representing a specific type of mineral are predominantly found to share similar pixel values (e.g. [5, 15, 21, 46, and 61]). Therefore, the self-similarity can be applied in order to classify the areas in which there are a huge number of pixels representing a specific mineral. Each class should be outlined by specific threshold values that are determined by the proposed method. According to Mandelbrot [27], a power-law relationship can be used to describe the relationship between the number of pixels,  $A_v$ , and the pixel values,  $P_v$ , as follows:

$$A_v = a (P_v)^{-\theta} \quad (3)$$

In the above equation,  $a$  is a constant factor, and  $\theta$  is the fractal dimension. In a log-log plot, Equation (3) is a linear relation. This means that the different straight lines plotted can be used to describe a class of similar pixels. The points connecting these lines can be used as the threshold values for the separation of different populations.

## 4. Results and Discussion

### 4.1. Robust principal component analysis

Robust principal components analysis is a method used to extract the important variables (as components) from the variables in a dataset. It actually extracts the low-dimensional features from a high-dimensional set to help register more information with fewer variables [21]. Consequently, the objective data becomes more meaningful. PCs result from merging the covariance matrix of  $X$  matrix data with  $n \times d$  dimension and  $X_i$  multivariable observations. It is necessary to determine the location  $T(x)$  and distributive estimator  $C(x)$  for the PCA transition. In the classical PCA,  $T(x)$  and  $C(X)$  are the arithmetic and distributive covariance matrices, respectively, which show the sensitivity to the outlier data. As a result, it is required to use other matrices like the minimum covariance determinant (MCD). This means that the data should be numerical and standardized [54]. In addition, it should be noted that the MCD estimator has been proposed based on the symmetry between the ellipsoids. There is a vital presumption before calculating RPCA, which states that the unprocessed data follow a multivariate normal distribution in the simplex space. In this method, an analysis is performed, where the bands that are very similar to each other are removed. In other words, by analysing and converting the bands using the eigenvalues and correlations, a new band is created using the new data that contains a huge amount of information. Therefore, the following steps should be taken to perform this method.

In order to reduce the image processing time, in one step, the important bands for each alteration were identified through the Crosta method, and then the RPCA analysis was performed. These methods have many similarities, in general, and are used to simplify the data structure. Also to explain the reason for using RPCA instead of PCA, a comparison was made between the two methods (Figure 2). The results of both methods show the dependence between the variables and the principal components. The details of these methods are available in many publications (e.g. [62, 63]).

The porphyry copper deposits are generally outlined by the broad halos of the phyllic, argillic, and propylitic alteration zones. The short wave infrared (SWIR) bands of ASTER are used for the delineation of the above-mentioned alterations. This is due to the fact that the minerals present in

these hydrothermal zones show a considerable absorption [4, 24, 64, and 65].

Illite and sericite, as the common mineral assemblages of phyllic alteration, show a strong absorption in the range of 2.2  $\mu\text{m}$ , which falls within the range of band 6 of Aster data while showing a significant reflection in band 7 [3]. Therefore, a combination of the bands 3, 5, 6, and 7 were used in PCA and RPCA for eliciting the traces of the phyllic alteration (Table 1).

As it can be seen in Table 1, the robust PC4 shows negative loadings for band 7 and band 3, while showing positive loadings for band 5 and band 6. Therefore, reversing the pixel values of robust PC4 (-PC4) yields a representation of the phyllic alteration (Figures. 2a and 2d). The bright pixels in the robust PC4 show the existing phyllic alteration.

**Table1. The results of RPCA method for identifying the phyllic alteration zone**

	PC <sub>1</sub>	PC <sub>2</sub>	PC <sub>3</sub>	PC <sub>4</sub>
<b>Band 3</b>	0.577486	0.396330	-0.654869	<b>-0.283867</b>
<b>Band 5</b>	0.549900	0.456604	0.655030	<b>0.245067</b>
<b>Band 6</b>	0.488132	-0.618626	-0.196809	<b>0.583348</b>
<b>Band 7</b>	0.354750	-0.501734	0.321479	<b>-0.720463</b>

In addition, according to a number of studies conducted [66], the bands 4, 5, 6, and 7 were selected for robust PCA in order to extract the features that show the argillic alteration (Table 2). The robust PC2 shows the absorption in the bands 5, 6, and 7, while showing reflection in band 4. Accordingly, the bright pixels in this robust PC show the existence of argillic alteration (Figures. 2b and 2e).

Turning to the propylitic alteration, a combination of bands representing epidote, chlorite, and calcite were used in RPCA to extract the traces of this alteration (Table 3). The robust PC2 appears to be the representative of this alteration. Figures 2c and 2f show the robust PC2 in which the bright pixels represent the propylitic alteration.

**Table2. The results of RPCA method for identifying the argillic alteration zone**

	PC <sub>1</sub>	PC <sub>2</sub>	PC <sub>3</sub>	PC <sub>4</sub>
<b>Band 4</b>	0.888063	<b>0.456369</b>	0.038411	0.039956
<b>Band 5</b>	0.284651	<b>-0.457377</b>	-0.349569	-0.766538
<b>Band 6</b>	0.270379	<b>-0.542342</b>	-0.472868	0.639653
<b>Band 7</b>	0.239194	<b>-0.537028</b>	0.807912	0.040820

**Table3. The results of RPCA method for identifying the propylitic alteration zone**

	PC <sub>1</sub>	PC <sub>2</sub>	PC <sub>3</sub>	PC <sub>4</sub>
<b>Band 4</b>	0.900428	<b>0.432163</b>	0.026928	0.041703
<b>Band 5</b>	0.288544	<b>-0.510723</b>	-0.268743	-0.763991
<b>Band 6</b>	0.274075	<b>-0.609757</b>	-0.374128	0.642735
<b>Band 8</b>	0.175654	<b>-0.424964</b>	0.887176	0.038352

After making the data robust to the classical principal component analysis, the results obtained indicate that the variables are well-distributed in the coordinate system of the binary diagram, which, in fact, expresses the structure of the open data in the real space. As illustrated in Figure 2, the images became sharp in the RPCA method. In other words, this method is more effective in improving the images due to the separation of background and sparse components. As it can be seen, this method is closer to the real data and has fewer errors.

#### 4.2. Application of pixel-value fractal model

The proposed methodology was applied for the classification of alteration zones, as delineated in Figure 2 (2a-2c). The log-log plots were drawn (Figures 3d-3f), and the cumulative number of pixels ( $A_v$ ) was plotted against the pixel values ( $P_v$ ). Four populations representing high intensity, medium intensity, low intensity, and background populations were delineated (Table 4). Figure 3 (3a-3c) presents the intensity distribution of the phyllic, argillic, and propylitic alteration zones.

**Table4. The result of C-A fractal method for alteration zones**

Alteration Zone	Background	Low intensity	Middle intensity	High intensity
Phyllic	0-128	128-152	152-202	202-255
Argillic	0-73	73-159	159-217	217-255
Propylitic	0-100	100-143	143-164	164-255

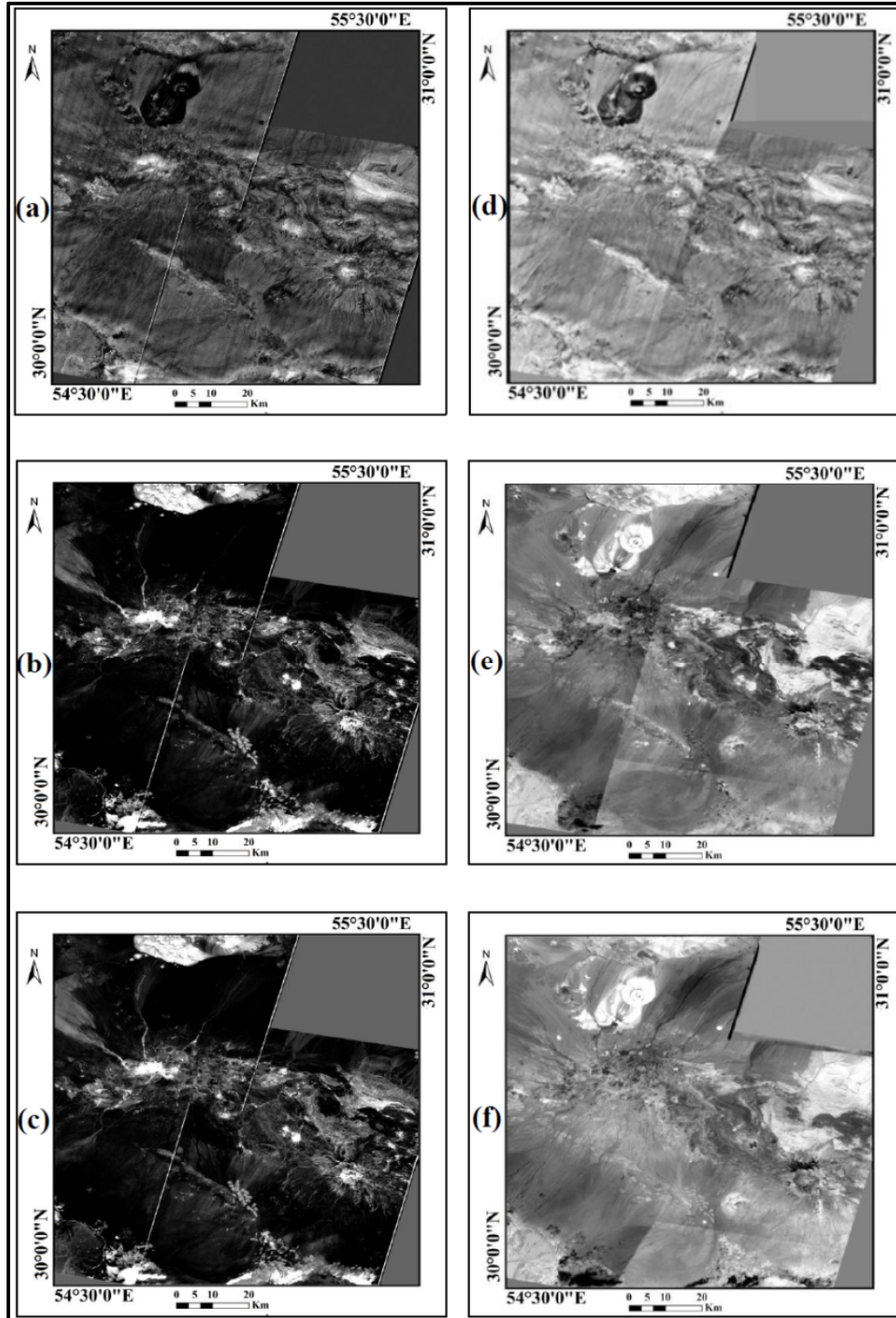


**Figure2. The bright pixels of map show (a) Phyllic, (b) Argillic, (c) Propylitic alteration by RPCA method - d, e and f by PCA method**

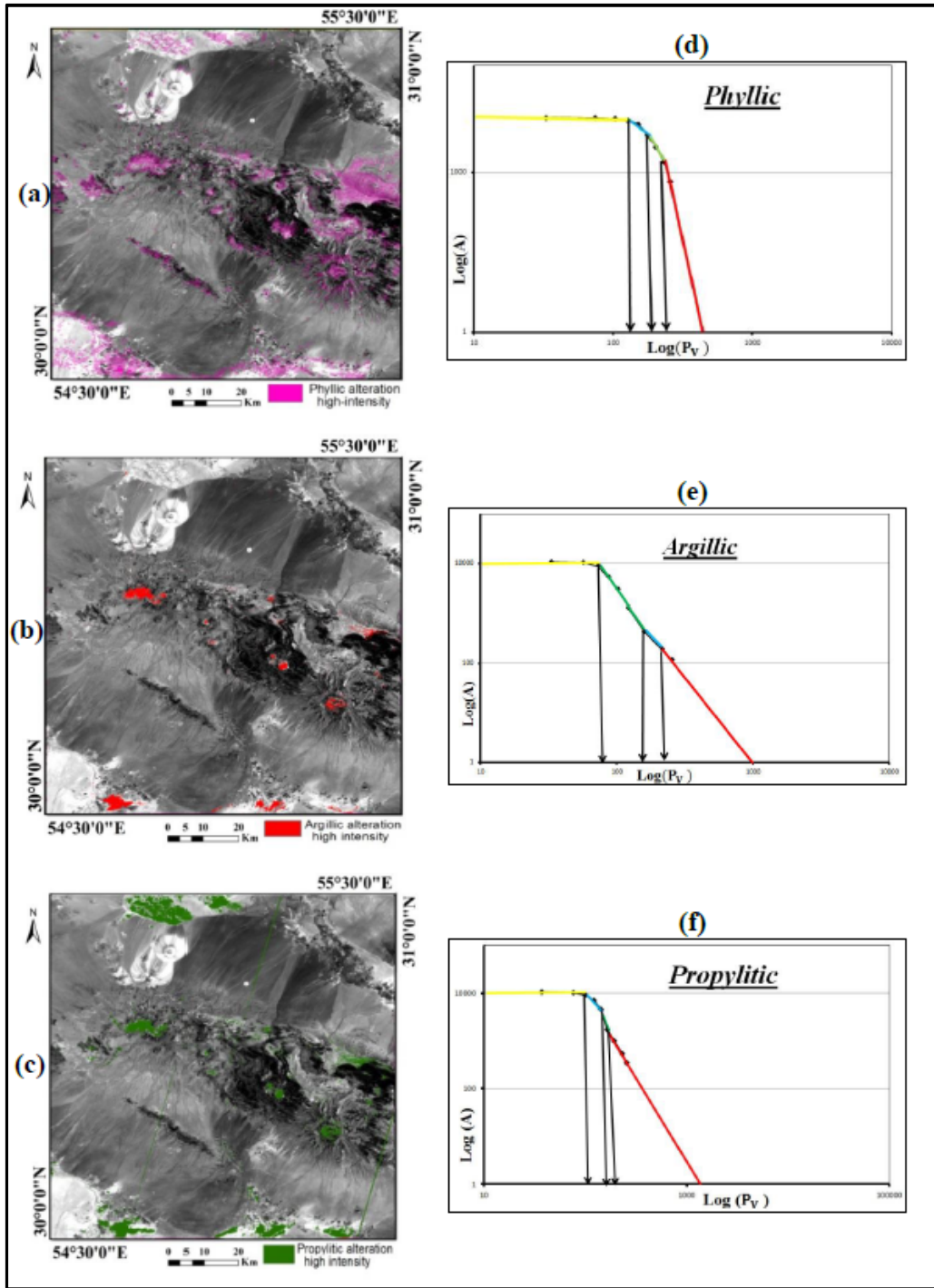


Figure 3. High intensity for (a) Phyllic, (b) Argillic and (c) Propylitic alteration maps and log-log diagrams, cumulative number of pixels ( $A_v$ ) and pixel values ( $P_v$ ) for (d) Phyllic, (e) Argillic, (f) Propylitic

### 4.3. Prediction-Area (P-A) plot

The purpose of validating a prediction model is to answer the question if one set of data is used to train the model (training data), and another set is used to validate the model (test data), will it be able to accurately predict the test data? In this work, in order to identify the efficient alterations,

we used the prediction-area (P-A) plot and normalized density ( $N_d$ ) because the alterations could be considered as the exploration targets. The alterations are controlled by adapting them to identify the mineral deposits in the studied area. Based on this description, the  $N_d$  coefficient can

be used to investigate the exploration targets [67]. This coefficient is defined as follows:

$$N_d = \frac{P_o}{P_a} \tag{4}$$

In the above equation,  $P_o$  is the ratio of the mineral deposit located in the exploration targets to total deposits, and  $P_a$  is the ratio of the area occupied by the exploration targets to the total area. In order to better represent the correlation between the exploration targets and the known mineral deposits, Equation (5) is shown logarithmically, and is called the effective weight ( $W_e$ ) [68, 69].

$$w_e = LnN_d \tag{5}$$

If  $W_e > 0$ , the selected targets are appropriate, and there will be a positive relationship between the selected targets and the known mineral deposits. If  $W_e \leq 0$ , there will be a negative relationship between the selected targets and the known mineral deposits.

We used the C-A method for distinguishing between the alterations. The P-A plot was drawn for the alteration layer (Figure 4). In order to calculate  $w_e$ , the intersection point of the diagram was extracted. In the studied area, the value of  $W_e$  for the alteration map is  $> 0$  and 1.39.

**4.4. Verification of results**

The field observations were conducted in the delineated zones. Twenty samples were randomly collected from the delineated highly intense

alteration zones (Figure 5). The samples were analyzed by the XRD technique (Table 5), revealing the existence of quartz in all samples. The samples collected from the argillic alteration show the significant existence of alunite and kaolinite (Table 5). Moreover, those taken from the phyllic alteration revealed a significant proportion of quartz, sericite, and pyrite. The analyzed samples show that the delineation of the alteration zones using the proposed methodology was successful.

The field observations coupled with the results of RPCA and pixel-value fractal model illustrate that the areas affected by the phyllic alteration are dominantly concentrated on the central part of the area (Figure 6). Nevertheless, the propylitic alteration is not merely constrained to the central zone, and is distributed in the central, northern, and southern parts of the area. The argillic alteration, however, can be observed in the southern and northern parts of the area. The correlation of the digital elevation model with the distribution of the argillic alteration reveals that this alteration dominantly occurs in the areas with a higher elevation. It is also imperative to note that phyllic is the most abundant alteration occurring in the studied area (Figs. 6).

The field studies and the performed sampling showed that the conducted study had a good performance in the delineation of the altered zones. Therefore, it is recommended to use the achieved maps for the exploration of further porphyry copper deposits.

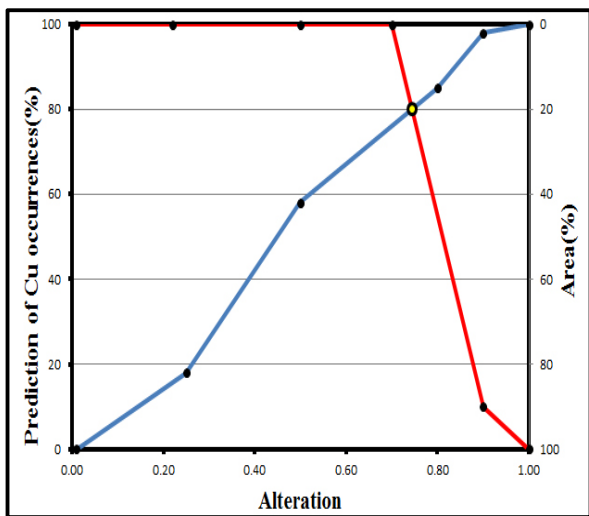


Figure4. P-A plot for alterations

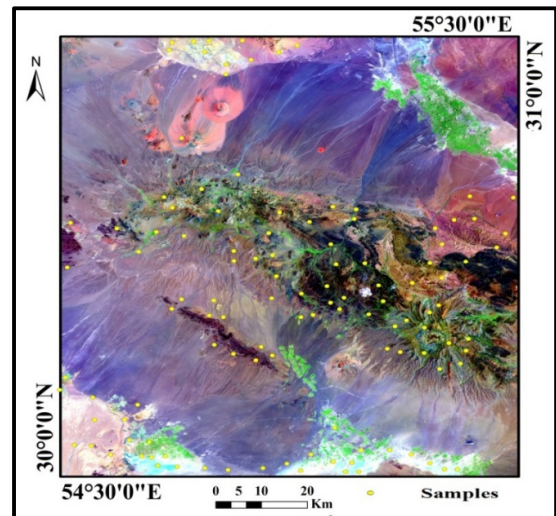


Figure5. False color composite image of the study area and sampling locations of hydrothermal alterations

Table 5. Results of XRD

No.	Minerals	No.	Minerals
9601	Quartz, Pyrophyllite, Rutile	9611	Quartz, Pyrophyllite, Alunite, Hematite, Calcite, Kaolinite
9602	Quartz, Jarosite, Kaolinite, Illite	9612	Quartz, Pyrophyllite, Goethite, Hematite, Kaolinite, Mica
9603	Quartz, Diaspore, Pyrophyllite, Mica, Illite, Kaolinite, Goethite, Hematite	9613	Epidote, Quartz, Alkali Feldspar
9604	Kaolinite, Quartz	9614	Quartz- Diaspore, Pyrophyllite, Kaolinite, Goethite, Hematite
9605	Kaolinite, Quartz, Natrolite	9615	Quartz, Mica, Illite
9606	Quartz, Goethite, Hematite	9616	Quartz, Illite, Goethite, Hematite, Chlorite, Pyrophyllite
9607	Quartz, Kaolinite, Alunite	9617	Quartz, Kaolinite, Pyrophyllite, Calcite, Hematite, Illite
9608	Quartz, Diaspore, Pyrophyllite, Illite, Mica, Illite, Goethite, Kaolinite	9618	Quartz, Pyrophyllite, Muscovite, Alkali Feldspar, Goethite
9609	Quartz, Pyrophyllite, Mica	9619	Quartz, Pyrophyllite, Goethite, Hematite, Alkali Feldspar
9610	Quartz, Mica, Illite	9620	Quartz, Pyrophyllite, Alkali Feldspar, Kaolinite

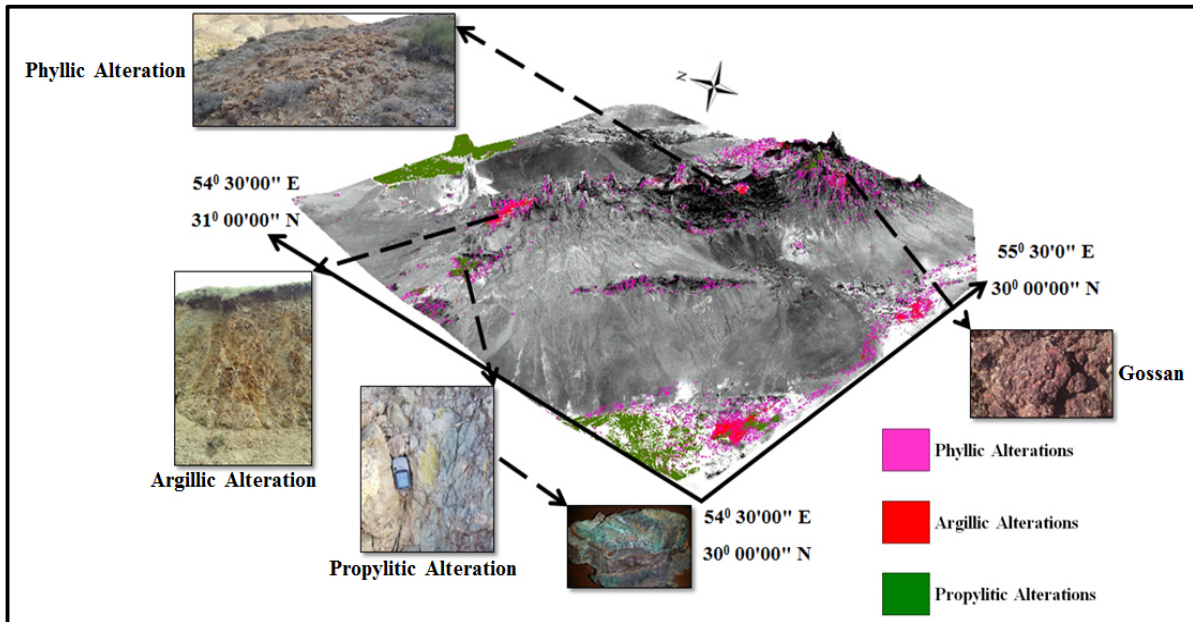


Figure 6. Digital elevation model map with some pictures from hydrothermal alterations in the field observation

5. Conclusions

In this work, we presented a novel methodology by combining the application of the robust principal component analysis (RPCA) and the proposed pixel-value fractal model for the delineation of porphyry copper-related alteration zones, phyllic, argillic, and propylitic alterations. Using the ASTER imagery data, it was revealed that the porphyry systems were developed in this area. In order to highlight the existence of this alteration, we used a selective approach in order to determine the bands incorporated into RPCA.

Three images were retrieved by the RPCA method, highlighting the distribution of the phyllic, argillic, and propylitic alterations. The images were compared by the PCA method. The alteration results are more accurate in the RPCA method rather than the PCA method, which appears to be due to the contrast and separation of background and sparse components. These images were subjected to a classification process using the proposed fractal procedure, which yielded four different classes of alteration zones including the high, medium, low, and very low intensities of the alterations. These methods are simple and

computationally easy, and therefore, a combination of the both techniques can be applied for mapping the alteration zones. In this area, the spatial distribution showed a northwest-southeast trend. Subsequently, the pixel-value method allowed reclassifying the alteration zones (propylitic, phyllic, and argillic). This method showed that the phyllic and argillic zones occurred in the center and were restricted by the propylitic zone. The intense zones were thus validated by the field observations. A total of 20 samples were collected from these zones, showing a high level of reliability. Also the P-A plot showed that the alterations had a positive relationship with the mineralization. It can, therefore, be concluded that the proposed methodology can be applied to different case studies for the delineation of the alteration zones.

## References

- [1]. Honarmand, M., Ranjbar, H. and Moezifar, Z. (2002). Integration and analysis of airborne geophysics, remote sensing and geochemical data of Sar Cheshmeh area using directed principal component analysis. *Exploration Mining Geology*. 11: 43–48.
- [2]. Ranjbar, H. and Honarmand, M. (2004). Integration and analysis of airborne geophysical and ETM+ data for exploration of porphyry type deposits in the Central Iranian Volcanic Belt using fuzzy classification. *International Journal of Remote Sensing*. 25: 4729–4741.
- [3]. Mars, J.C. and Rowan, L.C. (2006). Regional mapping of phyllic and argillic altered rocks in the Zagros magmatic arc, Iran, using Advanced Spaceborne Thermal Emission and Reflection Radiometer (ASTER) data and logical operator algorithms. *Geosphere*. 2 (3): 161-186.
- [4]. Tangestani, M. H., Mazhari, N., Agar, B. and Moore, F. (2008). Evaluating Advanced Spaceborne Thermal Emission and Reflection Radiometer (ASTER) data for alteration zone enhancement in a semi-arid area, northern Shahr-e-Babak, SE Iran. *International Journal of Remote Sensing*. 29: 2833–2850.
- [5]. Hosseinjani Zadeh, M. and Honarmand, M. (2017). A remote sensing-based discrimination of high-and low-potential mineralization for porphyry copper deposits; a case study from Dehaj-Sarduiyeh copper belt, SE Iran. *European Journal Remote Sensing*. 50 (1): 332-342.
- [6]. Saric, V. and Mijalkovic, N. (1973). Metallogenic map of Kerman region, 1:500000 scale. In: *Exploration for ore deposits in Kerman region*. Report No. 53, Tehran, Iran: Ministry of Economy Geological Survey of Iran.
- [7]. Waterman, G.C. and Hamilton, R.L. (1975). The Sar Cheshmeh porphyry copper deposit. *Economic Geology*. 70: 568–576.
- [8]. Shahabpour, J. and Kramers, J.D. (1987). Lead isotope data from the Sar Cheshmeh porphyry copper deposit. *Mineralium Deposita*. 22: 278–281.
- [9]. Hassanzadeh, J. (1993). Metallogenic and tectono-magmatic events in the SE sector of the Cenozoic active continental margin of Iran (Shahr-e-Babak area, Kerman province). Unpublished PhD thesis, University of California, USA.
- [10]. Ranjbar, H. (1996). An integrated study of remote sensing, geophysical and geochemical data in exploration for copper mineralization in the Pariz area, Kerman Province, Iran, with reference to GIS application. PhD thesis (unpublished), University of Delhi, India.
- [11]. Tangestani, M. and Moore, F. (2001). Comparison of three principal component analysis techniques to porphyry copper alteration mapping a case study in Meiduk area, Kerman, Iran. *Canadian Journal of Remote Sensing*. 27(2): 176–182.
- [12]. Tangestani, M.H. and Moore, F. (2002). Porphyry copper alteration mapping at the Meiduk area, Iran. *Journal of Remote Sensing*. 23: 4815–4825.
- [13]. McInnes, B.I.A., Evans, N.J., Fu, F.Q., Garwin, S., Belousova, E., Griffin, W.L., Bertens, A., Sukama, D., Permana Dewi, S., Andrew, R.L. and Deckart, K. (2005). Thermal history analysis of selected Chilean, Indonesian, and Iranian porphyry Cu–Mo–Au deposits. In: Porter, T.M. (Ed.), *Super Porphyry Copper and Gold Deposits: a Global Perspective*. Adelaide: PGC publishing.
- [14]. Shafiei, B. (2008). Metallogenic model for Kerman porphyry copper belt and its implications for exploration. PhD thesis (unpublished), Shaheed Bahonar University of Kerman, Iran.
- [15]. Safari, H., Bagas, L. and Shafiei Bafti, B. (2015). Structural controls on the localization of Cu deposits in the Kerman Cu metallogenic province of Iran using geoinformatic techniques. *Ore Geol. Rev.* 67: 43–56.
- [16]. Ayoobi, I. and Tangestani, M.H. (2017). Evaluating the effect of spatial subsetting on subpixel unmixing methodology applied to ASTER over a hydrothermally altered terrain. *International Journal of Applied Earth Observation and Geoinformation*. 62: 1–7.
- [17]. Safari, M., Maghsodi, A. and Pour, A.B. (2017). Application of Landsat-8 and ASTER satellite remote sensing data for porphyry copper exploration: a case study from Shahr-e-Babak, Kerman, south of Iran. *Geocarto International*. 32: 1-16.
- [18]. Lowell, J.D. and Guilbert, J.M. (1970). Lateral and vertical alteration-mineralization zoning in

porphyry ore deposits. *Economic Geology*. 65(4): 373–408.

[19]. Fakhari, S., Jafarirad, A., Afzal, P. and Lotfi, M. (2019). Delineation of hydrothermal alteration Zones for porphyry systems utilizing ASTER data in Jebal barez area, SE Iran. *Iranian Journal of Earth Sciences*. 11: 80-92.

[20]. Zamyad, M., Afzal, P., Pourkermani, M., Nouri, R. and Jafari, M.R. (2019). Determination of Hydrothermal Alteration Zones by Remote Sensing Methods in Tirka Area, Toroud, NE Iran. *Journal of the Indian Society of Remote Sensing*. 47: 1817–1830.

[21]. Afzal, P., Aramesh Asl, R., Adib, A. and Yasrebi, A.B. (2015). Application of Fractal Modelling for Cu Mineralisation Reconnaissance by ASTER Multispectral and Stream Sediment Data in Khoshname Area, NW Iran *Journal of the Indian Society of Remote Sensing*. 43: 121-132.

[22]. Crosta, A. P., Desouza Filhi, C. R., Azevedo, F. and Brodie, C. (2003). Targeting key alteration minerals in epithermal deposits in Patagonia, Argentina, using ASTER imagery and principal component analysis. *Journal of remote sensing*. 10: 4233–4240.

[23]. Kruse, F. A., Boardman, J. and Huntington, J. F. (2003). Comparison of airborne hyper spectral data and EO-1 Hyperion for mineral mapping. *IEEE Trans. Geoscience Remote Sensing*. 41: 1388–1400.

[24]. Rowan, L.C. and Mars, J.C. (2003). Lithologic mapping in the Mountain Pass, California, area using Advanced Spaceborne Thermal Emission and Reflection Radiometer (ASTER) data. *Remote Sens. Environ*. 84 (3): 350-366.

[25]. Hubbard, B. E. and Crowley, J. K. (2005). Mineral mapping on the Chilean–Bolivian Altiplano using co-orbital ALI, ASTER and Hyperion imagery: data dimensionality issues and solutions. *Remote Sensing Environment*. 99: 173–186.

[26]. Ducart, D. F., Crosta, A. P., Souza Filho, C. R. and Coniglio, J. (2006). Alteration mineralogy at the Cerro La Mina epithermal prospect, Patagonia, Argentina: field mapping, short-wave infrared spectroscopy, and ASTER images. *Economic Geology*. 101: 981–996.

[27]. Mandelbrot, B.B. (1983). *Fractal Geometry of Nature*, San Francisco: W.H. Freeman.

[28]. Dimitrijevic, M.D. (1973). *Geology of the Kerman region*. Report No. 52, Tehran, Iran: Ministry of Economy Geological Survey of Iran.

[29]. Khakzad, A. and Jaafari, H. (2002). Mineralogy and economic geology of copper deposits of Harare district in Kerman province. 10th Symposium of Crystallography and Mineralogy of Iran.

[30]. Zarasvandi, A., Pourkaseb, H. and Jalili, Y. (2016). Investigation on the relationship between copper mineralization in Khezr Abad and Shahrebabak area: regions: Using Fractal and fry analyzes. *Journal of Economic Geology*. 7: 385-402.

[31]. Daneshvar Saein, L. and Afzal, P. (2017). Correlation between Mo mineralization and faults using geostatistical and fractal modeling in porphyry deposits of Kerman Magmatic Belt, SE Iran. *Journal of Geochemical Exploration*. 181: 33-343.

[32]. Shafiei, B. (2010). Lead isotope signatures of the igneous rocks and porphyry copper deposits from the Kerman Cenozoic magmatic arc (SE Iran), and their magmatic–metallogenetic implications. *Ore Geol. Rev*. 38: 27–36.

[33]. Shafiei, B., Shamanian, Gh.H., Mathur, R. and Mirnejad, H. (2015). Mo isotope fractionation during hydrothermal evolution of porphyry Cu systems. *Mineralium Deposita*. 50: 281–291.

[34]. Alavi, M. (1994). Tectonics of Zagros orogenic belt of Iran, new data and interpretation. *Tectonophysics*. 229: 211–238.

[35]. Gupta, R.P. (2003). *Remote Sensing Geology*, Berlin: Springer.

[36]. Soe, M., Aung Kyaw, T. and Takashima, I. (2005). Application of remote sensing techniques on iron oxide detection from ASTER and Landsat images of tanintharyi coastal area Myanmar. *Akita University*. 26: 21-28.

[37]. Ahmadfaraj, M., Mirmohammadi, M. and Afzal, P. (2016). Application of fractal modeling and PCA method for hydrothermal alteration mapping in the Saveh area (Central Iran) based on ASTER multispectral data. *Int. J. Min. & Geo-Eng*. 50(1): 37–48.

[38]. Crosta, A. P. and Moore, J. M. (1989). Enhancement of Landsat Thematic Mapper imagery for residual soil mapping in SW Minas Gerais State, Brazil: a prospecting case history in Greenstone Belt Terrain. *Proceedings of the Seventh Thematic Conference on Remote Sensing for Exploration Geology*, 2–6 October, Calgary, Canada, ERIM, 1173–1187.

[39]. Abdelkareem, M. and El-Baz, F. (2017). Characterizing hydrothermal alteration zones in Hamama area in the central Eastern Desert of Egypt by remotely sensed data. *Geocarto International*. 1- 20.

[40]. Ruiz–Armenta, J. R. and Prol–Ledesma, R. M. (1998). Techniques for enhancing the spectral response of hydrothermal alteration minerals in Thematic Mapper images of central Mexico. *International Journal of Remote Sensing*. 19: 1981–2000.

[41]. Beiranvand Pour, A. and Hashim, M. (2012). The application of ASTER remote sensing data to porphyry

copper and epithermal gold deposits. *Journal of Ore Geology Reviews*. 44: 1–9.

[42]. Honarmand, M., Ranjbar, H. and Shahabpour, J. (2012). Application of Principal Component Analysis and Spectral Angle Mapper in the Mapping of Hydrothermal Alteration in the Jebal-Barez Area, Southeastern Iran. *Resource Geology*. 62(2): 119–139.

[43]. Shahriari, H., Ranjbar, H. and Honarmand, M. (2013). Image segmentation for hydrothermal alteration mapping using PCA and concentration-area fractal model. *Natural Resources Research*. 22 (3): 191–206.

[44]. Cheng, Q. and Li, Q. (2002). A fractal concentration-area method for assigning a color palette for image representation. *Computers and Geosciences*. 28: 567–575.

[45]. Carranza, E. J. M., Van Ruitenbeek, F. J. a., Hecker, C., Van der Meijde, M. and Van der Meer, F. D. (2008). Knowledge-guided data-driven evidential belief modeling of mineral prospectivity in Cabo de Gata, SE Spain. *International Journal of Applied Earth Observation and Geoinformation*. 10(3): 374–387.

[46]. Crosta, A. P., Desouza Filhi, C. R., Azevedo, F. and Brodie, C. (2003). Targeting key alteration minerals in epithermal deposits in Patagonia, Argentina, using ASTER imagery and principal component analysis. *Journal of remote sensing*. 24(21): 4233-4240.

[47]. Carranza, E. J. M. and Hale, M. (2002). Mineral imaging with Landsat Thematic Mapper data for hydrothermal alteration mapping in heavily vegetated terrance. *Journal of Remote Sensing*. 23(22): 4827-4852.

[48]. Honarmand, M., Ranjbar, H. and Shahabpour, J. (2011). Application of Spectral Analysis in Mapping Hydrothermal Alteration of the Northwestern Part of the Kerman Cenozoic Magmatic Arc, Iran. *University of Tehran, Journal of Sciences*. 22(3): 221-238.

[49]. Zoheir, B. and Emam, A. (2012). Integrating geologic and satellite imagery data for high-resolution mapping and gold exploration targets in the South Eastern Desert, Egypt. *Journal of African Earth Sciences*. 66-67: 22–34.

[50]. Qiu, J.T., Zhang, Ch. and Hu, X. (2015). Integration of Concentration-Area Fractal Modeling and Spectral Angle Mapper for Ferric Iron Alteration Mapping and Uranium Exploration in the Xiemisitan Area, NW China. *Remote Sensing*. 7: 13878-13894.

[51]. Parsa, M., Maghsoudi, A., Yousefi, M. and Sadeghi, M. (2016). Multifractal analysis of stream sediment geochemical data: Implications for hydrothermal nickel prospecting in an arid terrain, eastern Iran. *Journal of Geochemical Exploration*. 181: 305-317.

[52]. Rousseeuw, P.J. and Driessen, K.V. (1999). A fast algorithm for the minimum covariance determinant estimator. *Technometrics*. 41(3): 212-223.

[53]. Parsa, M., Maghsoudi, A., Carranza, E.J.M. and Yousefi, M. (2017a). Enhancement and mapping of weak multivariate stream sediment geochemical anomalies in Ahar Area, NW Iran. *Natural Resources Research*. 26(4): 443-455.

[54]. Buccianti, A. and Pawlowsky-Glahn, V. (2005). *New Perspective on Water Chemistry and Compositional Data Analysis*. *Mathematical Geology*. 37: 703-727, 2005.

[55] Zandiyyeh, F. (2007). Mineral exploration modeling of Cu and Mo deposits using litho-geochemical data in Iran (Sungun, Darrehzar and Ijo), MSc thesis (unpublished), Shaheed Bahonar University of Kerman, Iran.

[56]. Candes, E. J., Li, X., Ma, Y. and Wright, J. (2011). Robust principal component analysis. *Journal of the ACM*. 58(3):1–11.

[57]. Cheng, Q., Agterberg, F. P. and Ballantyne, S. B. (1994). The separation of geochemical anomalies from background by fractal methods. *Journal of Geochemical Exploration*. 51: 109-130.

[58]. Parsa, M., Maghsoudi, A., Yousefi, M. and Sadeghi, M. (2017c). Multifractal analysis of stream sediment geochemical data: Implications for hydrothermal nickel prospecting in an arid terrain, eastern Iran. *Journal of Geochemical Exploration*. 181: 305-317.

[59]. Parsa, M., Maghsoudi, A. and Yousefi, M. (2018). Spatial analyses of exploration evidence data to model skarn-type copper prospectivity in the Varzaghan district, NW Iran. *Ore Geology Reviews*. 92: 97-112.

[60]. Parsa, M. and Maghsoudi, A. (2018). Controls on Mississippi Valley-Type Zn-Pb mineralization in Behabad district, Central Iran: Constraints from spatial and numerical analyses. *Journal of African Earth Sciences*. 140: 189-198.

[61]. Ahmadfaraj, M., Mirmohammadi, M. and Afzal, P. (2016). Application of fractal modeling and PCA method for hydrothermal alteration mapping in the Saveh area (Central Iran) based on ASTER multispectral data. *International Journal Mining and Geo-Engineering*. 50: 37-48.

[62]. Tripathi, V.S. (1979). Factor analysis in geochemical exploration. *Journal of Geochemical Exploration*. 11(3): 263-275.

[63]. Jolliffe, I.T. (2002). *Principal component analysis*, John Wiley & Sons: Ltd.

[64]. Rowan, L. C., Schmidt, R. G. and Mars, J. C. (2006). Distribution of hydrothermally altered rocks in the Reko Diq, Pakistan mineralized area based on

spectral analysis of ASTER data. Remote Sensing of Environment. 104(1): 74–87.

[65]. Moore, F., Rastmanesh, F., Asadi, H. and Modabberi, S. (2008). Mapping mineralogical alteration using principal-component analysis and matched filter processing in the Takab area, north-west Iran, from ASTER data. International Journal of Remote Sensing. 29(10): 2851–2867.

[66]. Hunt, G. R. (1977). Spectral signatures of particulate minerals in the visible and near infrared. Geophysics. 42(3): 501–513.

[67]. Mihalasky, M.J. and Bonham-Carter, G.F. (2001). Lithodiversity and its spatial association with metallic

mineral sites, Great Basin of Nevada. Journal of Natural Resources Research. 10(3): 209-226.

[68]. Yousefi, M. and Carranza, E.J.M. (2015a). Fuzzification of continuous-value spatial evidence for mineral prospectivity mapping. Journal of Computers & Geosciences. 74: 97-109.

[69]. Yousefi, M. and Carranza, E.J.M. (2015b). Prediction-area (P-A) plot and C-A fractal analysis to classify and evaluate evidential maps for mineral prospectivity modeling. Journal of Computers & Geosciences. 79: 69–81.

## کاربرد آنالیز مولفه‌های اصلی مقاوم و فرکتال جهت جداسازی مناطق دگرسانی هیدروترمال مرتبط با کانی‌سازی با استفاده از داده‌های سنجنده ASTER: مطالعه موردی منطقه دهج- ایران مرکزی

نرگس حبیب خواه<sup>۱</sup>، حسین حسینی<sup>۱\*</sup>، عباس مقصودی<sup>۱</sup> و مهدی هنرمند<sup>۲</sup>

۱- دانشکده مهندسی معدن، دانشگاه امیرکبیر (پلی تکنیک)، تهران، ایران

۲- پژوهشکده علوم محیطی / گروه پژوهشی اکولوژی، دانشگاه تحصیلات تکمیلی صنعتی و فناوری پیشرفته، کرمان، ایران

ارسال ۲۰۲۰/۴/۲۷، پذیرش ۲۰۲۰/۹/۷

\* نویسنده مسئول مکاتبات: hhassani@aut.ac.ir

### چکیده:

منطقه دهج، در قسمت جنوبی کمربند ماگمایی ارومیه-دختر واقع شده که میزان تعدادی از کانسارهای مس پورفیری در مقیاس جهانی است. این کمربند شامل توالی آتشفشان - پلوتونیک اسیدی تا متوسط میزبانی مناسب می‌باشد که تحت تأثیر انواع مختلف دگرسانی گرمایی، اعم از آرژیلیک، فیلیک و پروپلیتیک قرار دارند. اگرچه تعداد زیادی از ذخایر مس پورفیری کشف شده در این منطقه وجود دارد، اما موقعیت زمین‌شناسی منطقه احتمال یافتن کانسارهای بیشتر را نشان می‌دهد. شناسایی و تعیین دگرسانی گرمایی می‌تواند راه را برای کشف مناطق بالقوه دیگری که احتمالاً میزبان ذخایر مس پورفیری هستند هموار کند. مطالعه حاضر با استفاده از تصاویر سنجنده ASTER و ترکیب روش کاهش ابعاد و کاربرد تکنیک‌های فرکتال یک روش ترکیبی جهت جداسازی مناطق دگرسانی گرمایی ارائه می‌دهد. به منظور کاهش ابعاد داده‌های چند باندهی ASTER و استخراج کانی‌های مربوط به دگرسانی گرمایی، از جمله ایلیت، سرسیت، کوارتز، کائولینیت، اپیدوت و کلریت از آنالیز مولفه اصلی مقاوم (RPCA) استفاده شد. با تأکید بر وجود مواد معدنی فوق‌الذکر، یکسری محدودیت‌ها برای جدا کردن مناطق تحت تأثیر دگرسانی گرمایی از بقیه واحدهای زمین‌شناسی و تفسیر آن مورد نیاز است. برای مقابله با چنین چالشی، نویسندگان برای اجزای اصلی استخراج شده روش فراکتال value-pixel را معرفی کردند. از روش (P-A) Prediction-Area جهت اعتبارسنجی استفاده شد و نشان داد که دگرسانی‌های شناسایی شده ارتباط معناداری با کانی‌زایی دارد همچنین نتایج با بررسی‌های زمین‌شناسی نیز تأیید شد. تعدادی نمونه از مناطق مشخص شده جمع‌آوری شده و نمونه‌ها با استفاده از تکنیک‌های XRD مورد تجزیه و تحلیل قرار گرفت و مشخص شد که این مطالعه در طبقه‌بندی مناطق دگرسانی گرمایی موفق عمل کرده است.

**کلمات کلیدی:** آنالیز مولفه‌های اصلی مقاوم، مدل فراکتال V-P، دگرسانی گرمایی، مس پورفیری.